X-ray Emission Spectroscopy of Single Protein Crystals Yields Insights into Heme Enzyme Intermediates

Sahand Emamian[1], Kendra A. Ireland[†,2], Vatsal Purohit[†,2], Kirklin L. McWhorter[2], Olga Maximova[3], Winter Allen[3], Scott Jensen[3], Diego M. Casa[4], Yulia Pushkar[3], Katherine M. Davis[2*]*

[1] Department of Physics, Emory University, Atlanta, GA 30322, USA

[2] Department of Chemistry, Emory University, Atlanta, GA 30322, USA

[3] Department of Physics and Astronomy, Purdue University, West Lafayette, IN 47907, USA

[4] Advanced Photon Source, Argonne National Laboratory, Lemont, IL 60439, USA

AUTHOR INFORMATION

Corresponding Author

*correspondence to: katherine.davis@emory.edu; ypushkar@purdue.edu

† These authors contributed equally.

Enzyme reactivity is often enhanced by changes in oxidation state, spin state, and metal-ligand covalency of associated metallocofactors. The development of spectroscopic methods for studying these processes coincidentally with structural rearrangements is essential for elucidating metalloenzyme mechanisms. Herein, we demonstrate the feasibility of collecting X-ray emission spectra of metalloenzyme crystals at a 3rd generation synchrotron source. In particular, we report the development of a von Hamos spectrometer for the collection of Fe Kβ emission optimized for analysis of dilute biological samples. We further showcase its application in crystals of the immunosuppressive heme-dependent enzyme indoleamine 2,3-dioxygenase. Spectra from protein crystals in different states were compared with relevant reference compounds. Complementary density functional calculations assessing covalency support our spectroscopic analysis and identify active site conformations that correlate to high- and low-spin states. These experiments validate the suitability of an X-ray emission approach for determining spin states of previously uncharacterized metalloenzyme reaction intermediates.

TOC GRAPHICS

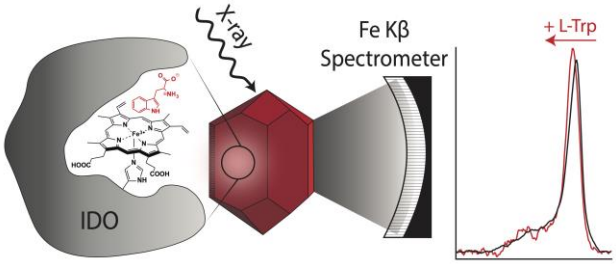

KEYWORDS metalloenzyme, spin, covalency, indoleamine 2,3-dioxygenase, iron, density functional theory, von Hamos

Metals are crucial to the biological processes of living organisms ranging from metabolism to transcriptional regulation and are incorporated into more than 40-50% of the proteome.[1] Enzymes, in particular, catalyze challenging chemical reactions by utilizing transition metal ions whose oxidation and spin states are coordinated with changes in atomic structure. While crystallographic studies are useful in determining the structural basis for enzyme reactivity, even time-resolved diffraction is insufficient for the characterization of metalloenzyme mechanisms as it provides little insight into the concerted redox changes that accompany catalysis. Complementary spectroscopic data is therefore essential. Moreover, electronic structure of the metal center must be monitored *in crystallo* for comparison to structural dynamics, as the kinetics may differ from those in solution.[2,3] Inner-shell X-ray spectroscopies are both compatible with crystallography and directly sensitive to the local electronic structure of the transition metal.[4-6] Furthermore, X-ray emission spectroscopy (XES) is adaptable for time-resolved studies as it can be collected in an energy dispersive manner, meaning a statistical representation of the full spectrum is obtained irrespective of the collection time.[7]

Promising preliminary studies combining the techniques have been attempted at hard X-ray free electron laser (XFEL) sources, but limited availability of these facilities combined with their ill-defined modes of radiation damage have hampered broad application.[8-10] To date, no transformative results have emerged, and the ability to evade X-ray-induced damage to sensitive metallocofactors is hotly debated. Fransson *et al.* describe the radiation-induced spectral effects on the Mn-containing metalloenzyme complex photosystem II as minimal up to flux densities of ~10^{11} photons/pulse with the beam focused to ~10 μm, conditions common to fs XFEL pulses.[11] However, Jensen *et al.* report more significant spectral changes that would interfere with data analysis and defeat the purpose of tandem spectroscopic measurements under similar conditions.[12]

The source of these changes was ascribed to a multi-photon absorption process at the metal ions which cannot be avoided by sample dilution or alterations to the metal ion environment. By contrast, other groups argue the prevalence of an alternative mechanism where solvated electrons generated in the process of X-ray absorption by atoms surrounding the metal ion can be as impactful in causing changes to metal electronic structure on an ultra-fast time scale.[13] It should be noted that the magnitude of spectral shifts can vary wildly depending on the element being probed and the average change in spin state, making any observable radiation-induced changes potentially problematic. To extend the application of XES to the broader enzymology community, this approach must become both more robust and more accessible. Synchrotron sources provide an ideal opportunity to achieve these goals as damage mechanisms are better characterized and experimental time more readily available.[14-17] Furthermore, most metalloenzyme kinetics do not require femtosecond resolution.[18-20]

Herein, we not only demonstrate the feasibility of collecting relevant XE spectra of metalloenzyme crystals using 3rd generation synchrotron sources, but further obtain insights into the heme-dependent human enzyme indoleamine 2,3-dioxygenase (IDO). IDO is a crucial component to metabolism of the amino acid L-tryptophan (L-Trp), catalyzing its conversion to N-formylkynurenine (NFK, Fig. 1A).[21] Together, L-Trp consumption and NFK production contribute to suppression of the immune system through multiple biochemical pathways, making IDO a key drug target in the treatment of disease, most notably cancer.[22-24] Despite its importance, a complete understanding of the mechanism remains elusive. The subtleties of even some stable intermediates, such as the reactant complex, have yet to be decoded. Particular ambiguity surrounds intermediate spin states and their origin. Herein, we demonstrate that XES can be added as an informative tool

to analyze this particular Fe-dependent enzymatic pathway, as well as other similar systems relevant for human health.

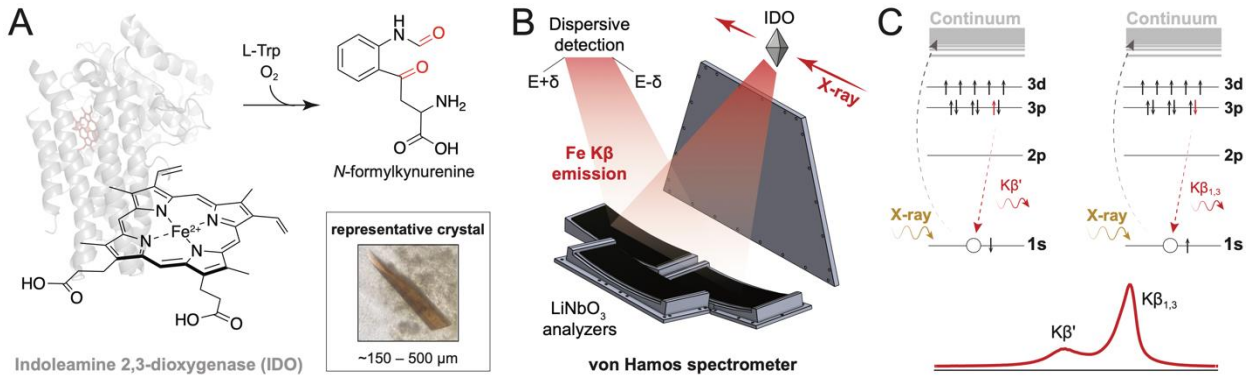

Figure 1. (A) IDO structure, reaction, and representative crystal used in this study. (B) Design schematic for Fe Kβ von Hamos spectrometer. (C) Pictorial depiction of electronic transitions following excitation of a core electron that give rise to the Kβ mainlines.

To both demonstrate broad applicability of the approach and observe electronic changes associated with the mechanistic behavior of IDO, we fabricated a new, wavelength-dispersive von Hamos spectrometer having an energy resolution of approximately 0.2 eV (see SI, Materials and Methods). Customizable design principles described previously were extended to develop the portable spectrometer in which three finely diced lithium niobate ($LiNbO_3$) analyzer crystals, arranged along a cylindrical curve, reflect emitted photons from 7012-7120 eV onto the surface of a pixel array detector (Fig. 1B).[25] This energy range encompasses Fe Kβ fluorescence, for which the most intense spectral lines correspond to photon emission from 3*p* to 1*s* transitions following excitation of an electron from the innermost shell, as well as the valence-to-core region corresponding to ligand orbital to 1*s* transitions not discussed in this report. In first row transition metals, coupling between the resultant unpaired 3*p* electron and the valence shell splits the main Kβ peak in two ($Kβ_{1,3}$ and the weaker satellite, Kβ′), thereby generating a powerful sensitivity to

spin and, to a lesser extent, effective nuclear charge (Fig. 1C). More precisely, the greater the number of unpaired 3*d* electrons, the more substantial the 3*p*-3*d* exchange interaction.[26, 27]

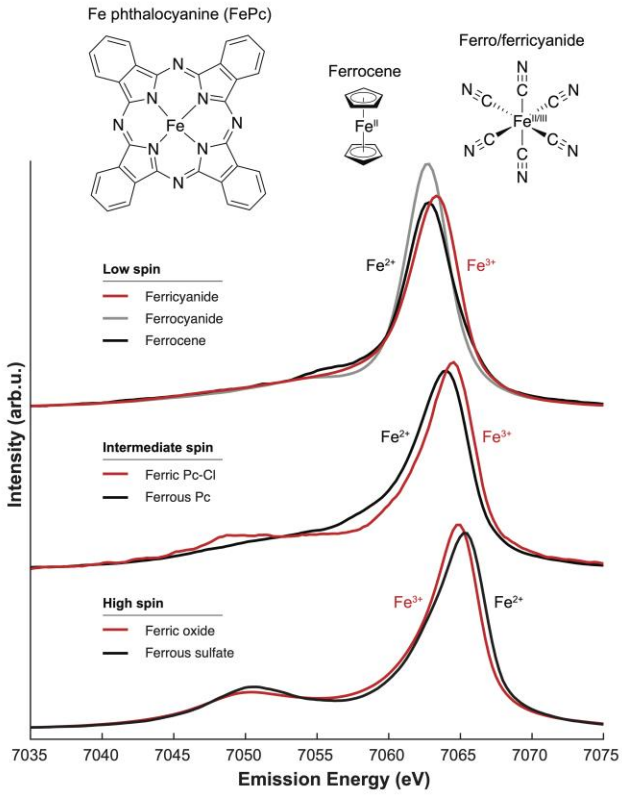

Figure 2. Emission spectra for a series of Fe standards demonstrate changes in peak position and shape due to oxidation and spin state. Spectra were normalized by the integral of the mainline peaks (see SI for more information).

The spectrometer was commissioned at the Advanced Photon Source of Argonne National Laboratory. To assess its performance, we collected XE spectra for seven, primarily mononuclear Fe, model compounds (Fig. 2). In addition to visual inspection, quantification of changes in peak position were analyzed through comparison of first moments (i.e. intensity-weighted average emission energies, Table 1). Early XES experiments demonstrated that distinguishing between oxidation states of Fe via Kβ main line analysis is particularly challenging.[28, 29] Despite an increase

in the number of unpaired *d* electrons in ferric complexes, associated increases in metal-ligand covalency often obscure expected changes to the magnitude of peak splitting.[29, 30]

Table 1. Characteristics of Fe complexes from formal, spectral, and computational analysis.

Name	Spin State	Nominal Spin	Spin Density[a]	IAD	IAD-Spin	1st Moment (eV)	% Covalency[b]
Ferric oxide	HS	2.5	2.40	0.55	–	7064.56	18.4
Ferrous sulfate	HS	2	2.18	0.64	–	7064.83	7.0
Fe(III)Pc-Cl	mix	~1.85	1.69	0.49	1.75	7063.73	32.6
Fe(II)Pc	IS	~1	1.04	0.37	1.25	7064.25	33.7
Ferricyanide	LS	0.5	0.48	0.19	–	7063.30	55.6
Ferrocyanide	LS	0	0	0	–	7062.79	58.6
Ferrocene	LS	0	0	0.15	–	7062.99	51.6
Ferrous IDO	HS[c]	2[c]	2.02	0.49	1.77	7064.34	23.3
Ferric IDO	mix	~1.5	1.54	0.48	1.73	7064.46	23.9
Ferric IDO + W	mix	~1.26	1.22	0.38	1.30	7063.88	34.9

[a]DFT-derived spin densities, corrected using the fit in Fig. S2. [b]Percent covalency for the Fe standards was determined via QRO methods, while IDO covalency values were predicted from the reference curve in Fig. S2. [c]Spin state may differ at low temperatures. See SI for computational details and DFT coordinates (Fig. S3-S4 and Tables S2-S15).

While differences between spectra of ferrous and ferric complexes having similar spin states are small, they are clearly detectable with our setup. Low-spin (LS) and intermediate-spin (IS) compounds follow expected trends in which the increasing spin state upon oxidation results in greater splitting and a shift of $K\beta_{1,3}$ to higher energies (Table 1, Fig. 2). Spectra of the selected high-spin (HS) compounds, by contrast, depict a decrease in splitting upon oxidation. This effect can be rationalized by the increased covalency of ferric oxide compared to ferrous sulfate heptahydrate due to the presence of comparatively stronger field ligands (O^{2-} versus water). The degree of covalency and iron d-orbital spin density (Table 1) can be further simulated with quasi-restricted orbitals (QROs) [31, 32] developed from density functional theory (DFT). More specifically, we calculate the degree of *d*-orbital character, which is simply a measure of the deviation of the

molecular orbital (Löwdin) population from that of a free ion. Its complement (100 – *d*-orbital character) is therefore also a measure of covalency, as the ligand reduces the electronic population of the orbitals.[32] It is important to note, however, that this approach to evaluating covalency was developed for application to octahedral and tetrahedral complexes and may not be as reliable for disparate geometries, such as five-coordinate ferrous IDO. From our QRO analysis, ferric oxide has more significant covalent interactions with its ligands, indicated by an 11.4% reduction in *d*-orbital character compared to ferrous sulfate heptahydrate. This enhanced hybridization of the Fe 3*d* orbital lowers the spin polarization density of the complex, redistributing Kβ′ intensity and negating the effects of increased spin.

Spectral shifts associated with changing spin state are more significant, ranging from 1-2 eV (Table 1), in agreement with other studies, and are accompanied by a concomitant reduction in Kβ′ peak intensity for LS Fe (Fig. 2).[33, 34] To establish a more systematic and quantitative correlation between changes in spin state and peak position, we calculated integrated absolute differences (IADs) with respect to the spectrum of ferrocyanide. IADs have been demonstrated to vary linearly with spin, and a reference curve was generated using a subset of the complexes for which nominal spin states are well-characterized (see Figure S1, and see SI for methods).[35] With our choice of reference spectrum, a greater experimentally-determined IAD correlates to a greater spin state.[28]

This type of analysis is particularly relevant for the study of species with unknown and/or complex spin states, such as those inherent to metalloenzyme intermediates. For example, calculated IAD values can be used to predict the spin of our selected Fe phthalocyanine samples. Intriguingly, the most accurate prediction is obtained for ferric phthalocyanine chloride ($S = 1.75$), which has been determined from magnetic susceptibility studies to be an admixture of IS and HS species ($S = 1.85$).[36, 37] The IAD-derived spin of ferrous phthalocyanine, by contrast, is 1.25, 25%

greater than that measured experimentally.[38, 39] It is unclear whether this discrepancy originates in the applied analysis or as-of-yet undetected subtleties of the ferrous phthalocyanine IS complex. Nonetheless, with an average deviation from known spins of approximately 15%, we were confident in our approach.

We therefore began working with single crystals of IDO. Data collection was attempted with both 'continuous' monochromatic and pulsed pink beam sources to assess the feasibility of future time-resolved measurements (see the SI for details). Due to time constraints associated with obtaining sufficient signal to differentiate the small shifts associated with changes in the effective nuclear charge, we opted to focus on elucidating spin states. The corresponding spectral changes are not only more significant, making them easier to detect, but spin states are also dominated by ligand field effects. Assuming that the Fe-coordination environment changes more slowly as a function of the X-ray dose, this characteristic of metalloenzyme complexes should be less sensitive to X-ray-induced damage. XE spectra were collected for ferric and ferrous IDO as well as ferric IDO in the presence of its substrate L-Trp.

Not only is our spectrometer capable of attaining sufficient signal-to-noise to visualize the Kβ mainlines of IDO crystals following excitation, but we further observe a shift in the $K\beta_{1,3}$ first moment of approximately -0.58 eV upon complexation of ferric IDO with L-Trp (Fig. 3). Such a redshift suggests a decrease in spin state and positions the associated $K\beta_{1,3}$ peak closer to the LS ferrocyanide standard. By contrast, the $K\beta_{1,3}$ peak of ferrous IDO all but overlays with the spectrum of ferric IDO (Fig. 3). First moment analysis yields a shift of only +0.12 eV, placing both spectra directly adjacent to the HS standard. From a redox perspective, alignment of the ferrous and ferric complexes is not particularly surprising given that the X-ray dosage applied to these samples (see Table S1) has been shown to reduce ferric heme in other proteins,[17] and spectral shifts

due to changes in effective nuclear charge are small.[30] However, the cryogenic conditions of the experiment would likely prevent any large-scale structural changes that could dramatically affect the Fe-coordination environment and thus its respective spin states. Altogether, observed changes in spectral position are consistent with previous experimental spin state analysis. And, to the best of our knowledge,[10] the associated XE spectra of ferric IDO are the first to differentiate between spin states of metalloenzyme crystals having the same formal oxidation state.

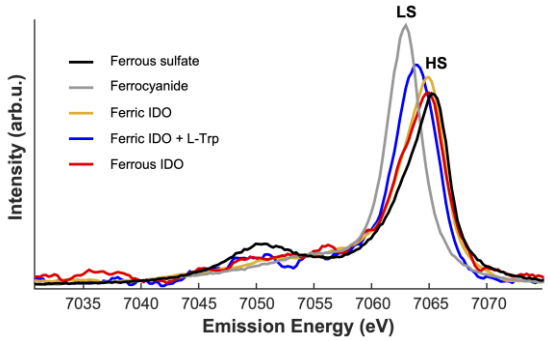

Figure 3. Emission spectra from single crystals of different IDO complexes compared to ferrous standards. Data were collected at 100 K.

Ferric IDO is known to be a pH-dependent mixture of HS (S = 5/2) and LS (S = 1/2) heme, and previous studies have estimated the ratio of HS to LS species to be roughly equal at pH 6.6.[40, 41] Prior to structural characterization of the enzyme,[42] the identities of these HS and LS components were hypothesized to be histidine/water (Fig. 4A) and bisnitrogenous coordinated heme, respectively.[41] Given the lack of a suitable distal histidine ligand, however, we propose that 3*p*-3*d* exchange is instead mitigated by altered positioning of an active site loop (Fig. 4B, chains A & C from PDB ID 6E44), which promotes heme coordination by the carbonyl group of an active site alanine (Ala264).[43] Upon addition of substrate, the spin state equilibrium shifts toward greater LS character, theorized to correspond to hydroxide-bound heme that is hydrogen-bonded to the

pyrrolic nitrogen of L-Trp (Fig. 4C).[44] This ligand-dependent spin crossover is supported further by previous XES studies on metal-organic frameworks.[45]

Papadopoulou *et al.* estimated a ligand distribution of approximately 33/7/60 (X/water/hydroxide) in the presence of L-Trp at pH 8, where X represents an active site residue, such as Ala264.[41] Persistence of alanine coordination, and the associated steric constraints on the distal face of the heme cofactor, may help to explain ferric IDO's relatively low affinity for L-Trp.[43]

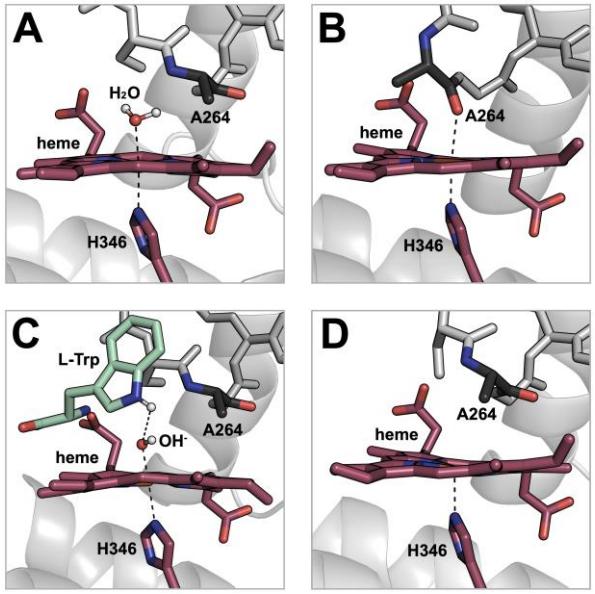

Figure 4. Active site configurations for various states of IDO. (A) Ferric IDO with water coordinated to the metal ion (PDB ID: 6E40). The water pictured was added *in silico* based on the DFT-optimized position (Table S13). (B) Ferric IDO with Ala264 coordinated to the metal ion (PDB ID: 6E44). (C) Ferric IDO with hydroxide coordinated to the metal ion and L-Trp bound in the active site (PDB ID: 6E35). Cyanide was removed from 6E35 and replaced by hydroxide in the DFT-optimized position for visualization (Table S11). (D) Five-coordinate ferrous IDO (PDB ID: 6E45).

To more rigorously assess the origin of associated LS components, we performed DFT optimizations and QRO spin analysis on truncated models of the IDO active site generated from published crystallographic models (Tables S10-S15).[43] In the absence of substrate, models depicting coordination by Ala264 (Table S14) returned the lowest energy values when heme was in a LS state (Table S15). Similar behavior was observed upon *in silico* addition of a hydroxide ion in the presence of L-Trp (Tables S11 & S15). Moreover, absence of the coordinating hydroxide ion led to a staggering 62.6 kcal/mol increase in the calculated energy of the substrate-bound complex. Together, these results stand in support of both hypotheses described above: (1) introduction of LS character in the absence of substrate occurs due to coordination by an active site alanine, and (2) upon L-Trp binding to the HS form of the ferric enzyme, associated deprotonation of the coordinating water lends additional LS character to the bulk sample.

Our ferric IDO crystals were generated at pH ~6.5 (see the SI), and thus, based on the heme populations observed by Papadopoulou *et al.* at this pH,[40] we expect an approximately 50/50 ratio of HS/LS heme in the absence of substrate. This mixture of spin states is qualitatively reflected by the intensity of the observed Kβ′ peak, which is weaker than is typical for purely HS complexes. Despite accounting for the presence of substantial LS character in our ferric IDO samples, however, the spectral shift upon addition of substrate remains quite modest in comparison to spin state related shifts reported for Fe standards. Based on the position of the relevant $K\beta_{1,3}$ peak, it seems likely that our ferric IDO crystals co-crystallized in the presence of L-Trp contain significant HS contamination relative to the Papadopoulou *et al.* study. This result is not unexpected, as lower pH also enhances the HS character for ferric IDO without L-Trp bound. Conveniently, we can estimate the relative HS and LS populations to a first order approximation, through application of the Henderson-Hasselbach equation, with the HS population corresponding to the water-bound

state and the LS populations corresponding to the hydroxide-bound and Ala264 coordinated states. This analysis yields a modified ligand distribution of approximately 38/38/24 (Ala264/water/hydroxide) for samples generated at pH 6.5, assuming the 1:1 ratio of water-to-alanine ligation is maintained in the presence of substrate (see the SI). Excitingly, we can closely reproduce these experimentally estimated spin state distributions via our IAD reference curve.

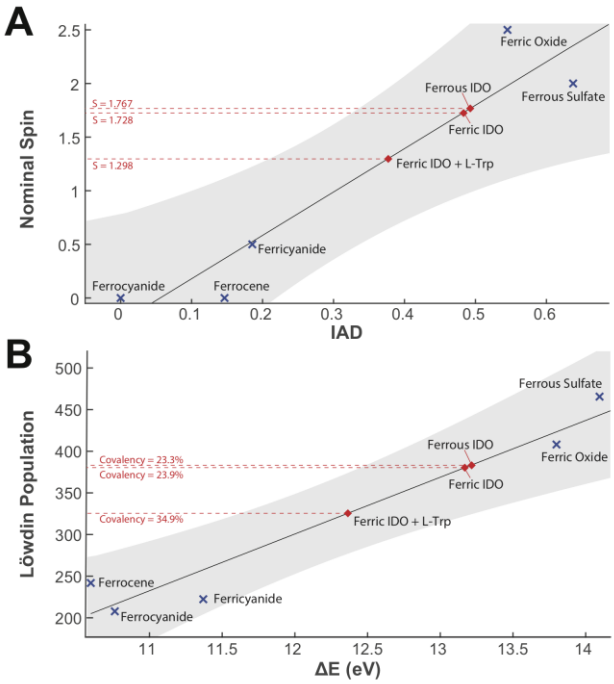

Figure 5. (A) IAD analysis based on a reference curve generated from a set of known spin state Fe standards (see Fig. S1). Grey shading indicates 95% confidence interval of fit. (B) Similar covalency analysis based on a comparison of $K\beta_{1,3}$ and $K\beta'$ peak splitting and DFT orbital population calculations.

Calculated IAD values correlate to spins of 1.73 and 1.30 for ferric IDO and ferric IDO with L-Trp bound, respectively (Fig. 5A, Table 1), suggesting an approximate error of 9%. Similar correlations can be made between the *d*-orbital character of the metallocofactor and the splitting of the IDO mainline peaks (see the SI). This covalency analysis depicts trends that match ones obtained using IADs (Fig. 5B, Table 1). Ferrous and ferric IDO samples had very similar IAD-

calculated spin states, which conform well to their independently calculated covalencies (23% and 24%, respectively). Conversely, ferric IDO with L-Trp bound has lower nominal and calculated spin states, which correspond to the high calculated covalency (35%).

Analysis of the ferrous IDO spin state can be approached in a similar way, beginning with visual comparison of the IDO and ferrous sulfate $K\beta_{1,3}$ peak positions. This qualitative analysis would appear to suggest substantial HS character in crystals of the ferrous enzyme, in agreement with earlier room temperature resonance Raman, MCD, and UV-vis absorbance studies that observed spectral features consistent with a five-coordinate HS heme cofactor.[40, 44, 46] X-ray crystallographic models depicting the ferrous enzyme further support this proposal, as the loop containing Ala264 does not directly interact with the metal ion, and no alternative distal ligand is identified (Fig. 4D).[43, 47, 48] However, the intensity and shape of the ferrous IDO Kβ' peak is more consistent with an IS or LS complex. We hypothesize that LS character may be introduced, at least in part, due to the cryogenic conditions (100 K) under which these data were collected, as has been inexplicably observed for other water/histidine-coordinated heme complexes.[41, 49] Such behavior can likewise be employed to rationalize overlap with the ferric IDO spectrum, suggesting an upper bound of 25% LS contamination. Our IAD-predicted spin (S = 1.77) for the ferrous form of the enzyme further validates this hypothesis and would correlate to ~89% HS character (Fig. 5A). The calculated covalency values also corroborate these findings: ferric IDO bound to L-Trp has the highest covalency, which depresses the spin state below those of ferrous and ferric IDO. While the integer spin states of ferrous complexes are difficult to confirm directly, our XE spectra provide clear evidence in support of a predominantly HS assignment, even at low temperatures.

In conclusion, the studies presented herein serve as a proof-of-concept for the collection of XE data of metalloenzyme crystals at 3rd generation synchrotron sources. Our analysis not only

confirms that XES provide novel insights into complex metalloenzyme spin state equilibria, but further that this analysis can tolerate a degree of radiation-induced damage. Paired with time-resolved techniques, this methodology lends itself well to tracking intermediates of enzyme turnover, which typically include spin- and oxidation-state changes. With many facilities upgrading to 4^{th} generation capabilities, having 10^3 times the photon flux, the feasibility of these and future time-resolved experiments can only improve.[50, 51]

ASSOCIATED CONTENT

Supporting Information. The following files are available free of charge.

Materials and methods, Figures S1-S4, Tables S1-S15. (PDF)

AUTHOR INFORMATION

Notes

† These authors contributed equally.

The authors declare no competing financial interests.

ACKNOWLEDGMENTS

This research was supported by the National Institutes of Health Pathway to Independence Award 4R00GM129460 (K.M.D.), the Beckman Young Investigator Program (K.M.D.), and Emory University start-up funds (K.M.D.). Additional support was provided by the National Science Foundation (NSF) under Grant No. CHE-2155060 (Y.P.) and the NSF Graduate Research Fellowship Program under Grant No. 1937971 (K.A.I.). Any opinions, findings, and conclusions or recommendations expressed in this material are those of the author(s) and do not necessarily

reflect the views of the National Science Foundation. This research used resources of the Advanced Photon Source, a U.S. Department of Energy (DOE) Office of Science User Facility operated by Argonne National Laboratory under Contract No. DE-AC02-06CH11357. Sector 20 is also supported by the Canadian Light Source and its funding partners, while BioCARS is also supported by the National Institute of General Medical Sciences of the National Institutes of Health under grant number P41 GM118217. We are grateful to Shelly Kelly and Chengjun Sun at Sector 20 of the Argonne National Laboratory for their assistance with data collection and experimental setup. We additionally thank Jamal Musaev and Alex Kaledin at Emory University's Cherry L. Emerson Center for Scientific Computation for assistance with DFT calculations.

REFERENCES

(1) Chen, A. Y.; Adamek, R. N.; Dick, B. L.; Credille, C. V.; Morrison, C. N.; Cohen, S. M. Targeting Metalloenzymes for Therapeutic Intervention. *Chem. Rev.* **2019**, *119* (2), 1323-1455.

(2) Spilburg, C. A.; Bethune, J. L.; Vallee, B. L. Kinetic Properties of Crystalline Enzymes. Carboxypeptidase A. *Biochemistry* **1977**, *16* (6), 1142-1150.

(3) Doscher, M. S.; Richards, F. M. The Activity of an Enzyme in the Crystalline State: Ribonuclease S. *J. Biol. Chem.* **1963**, *238* (7), 2399-2406.

(4) Glatzel, P.; Bergmann, U. High Resolution 1s Core Hole X-ray Spectroscopy in 3d Transition Metal Complexes—Electronic and Structural Information. *Coord. Chem. Rev.* **2005**, *249* (1), 65-95.

(5) Kern, J.; Tran, R.; Alonso-Mori, R.; Koroidov, S.; Echols, N.; Hattne, J.; Ibrahim, M.; Gul, S.; Laksmono, H.; Sierra, R. G.; et al. Taking Snapshots of Photosynthetic Water Oxidation Using Femtosecond X-ray Diffraction and Spectroscopy. *Nat. Commun.* **2014**, *5*, 4371-4381.

(6) Kowalska, J.; DeBeer, S. The Role of X-ray Spectroscopy in Understanding the Geometric and Electronic Structure of Nitrogenase. *Biochim. Biophys. Acta* **2015**, *1853* (6), 1406-1415.

(7) Davis, K. M.; Sullivan, B. T.; Palenik, M. C.; Yan, L.; Purohit, V.; Robison, G.; Kosheleva, I.; Henning, R. W.; Seidler, G. T.; Pushkar, Y. Rapid Evolution of the Photosystem II Electronic Structure During Water Splitting. *Phys. Rev. X.* **2018**, *8* (4), 41014-41024.

(8) Fransson, T.; Chatterjee, R.; Fuller, F. D.; Gul, S.; Weninger, C.; Sokaras, D.; Kroll, T.; Alonso-Mori, R.; Bergmann, U.; Kern, J.; et al. X-ray Emission Spectroscopy as an in Situ Diagnostic Tool for X-ray Crystallography of Metalloproteins Using an X-ray Free-Electron Laser. *Biochemistry* **2018**, *57* (31), 4629-4637.

(9) Alonso-Mori, R.; Kern, J.; Gildea, R. J.; Sokaras, D.; Weng, T.-C.; Lassalle-Kaiser, B.; Tran, R.; Hattne, J.; Laksmono, H.; Hellmich, J.; et al. Energy-Dispersive X-ray Emission Spectroscopy Using an X-ray Free-Electron Laser in a Shot-by-Shot Mode. *Proc. Natl. Acad. Sci.* **2012**, *109* (47), 19103-19107.

(10) Bergmann, U.; Kern, J.; Schoenlein, R. W.; Wernet, P.; Yachandra, V. K.; Yano, J. Using X-ray Free-Electron Lasers for Spectroscopy of Molecular Catalysts and Metalloenzymes. *Nat. Rev. Phys.* **2021**, *3* (4), 264-282.

(11) Fransson, T.; Alonso-Mori, R.; Chatterjee, R.; Cheah, M. H.; Ibrahim, M.; Hussein, R.; Zhang, M.; Fuller, F.; Gul, S.; Kim, I. S.; et al. Effects of X-ray Free-Electron Laser Pulse Intensity on the Mn Kβ1,3 X-ray Emission Spectrum in Photosystem II - A Case Study for Metalloprotein Crystals and Solutions. *Struct. Dyn.* **2021**, *8* (6), 64302-64315.

(12) Jensen, S. C.; Sullivan, B.; Hartzler, D. A.; Aguilar, J. M.; Awel, S.; Bajt, S. a.; Basu, S.; Bean, R.; Chapman, H. N.; Conrad, C.; et al. X-Ray Emission Spectroscopy at X-Ray Free

Electron Lasers: Limits to Observation of the Classical Spectroscopic Response for Electronic Structure Analysis. *J. Phys. Chem. Lett.* **2019**, *10* (3), 441-446.

(13) Blachucki, W.; Kayser, Y.; Czapla-Masztafiak, J.; Guo, M.; Juranic, P.; Kavcic, M.; Kallman, E.; Knopp, G.; Lundberg, M.; Milne, C.; et al. Inception of Electronic Damage of Matter by Photon-Driven Post-Ionization Mechanisms. *Struct. Dyn.* **2019**, *6* (2), 24901-24908.

(14) Davis, K. M.; Kosheleva, I.; Henning, R. W.; Seidler, G. T.; Pushkar, Y. Kinetic Modeling of the X-ray-Induced Damage to a Metalloprotein. *J. Phys. Chem. B* **2013**, *117* (31), 9161-9169.

(15) Weik, M.; Ravelli, R. B.; Kryger, G.; McSweeney, S.; Raves, M. L.; Harel, M.; Gros, P.; Silman, I.; Kroon, J.; Sussman, J. L. Specific Chemical and Structural Damage to Proteins Produced by Synchrotron Radiation. *Proc. Natl. Acad. Sci.* **2000**, *97* (2), 623-628.

(16) de la Mora, E.; Coquelle, N.; Bury, C. S.; Rosenthal, M.; Holton, J. M.; Carmichael, I.; Garman, E. F.; Burghammer, M.; Colletier, J.-P.; Weik, M. Radiation Damage and Dose Limits in Serial Synchrotron Crystallography at Cryo- and Room Temperatures. *Proc. Natl. Acad. Sci.* **2020**, *117* (8), 4142-4151.

(17) Pfanzagl, V.; Beale, J. H.; Michlits, H.; Schmidt, D.; Gabler, T.; Obinger, C.; Djinović-Carugo, K.; Hofbauer, S. X-ray–Induced Photoreduction of Heme Metal Centers Rapidly Induces Active-Site Perturbations in a Protein-Independent Manner. *J. Biol. Chem.* **2020**, *295* (39), 13488-13501.

(18) Kryatov, S. V.; Rybak-Akimova, E. V.; Schindler, S. Kinetics and Mechanisms of Formation and Reactivity of Non-Heme Iron Oxygen Intermediates. *Chem. Rev.* **2005**, *105* (6), 2175-2226.

(19) Huang, X.; Groves, J. T. Oxygen Activation and Radical Transformations in Heme Proteins and Metalloporphyrins. *Chem. Rev.* **2018**, *118* (5), 2491-2553.

(20) Bruice, T. C.; Benkovic, S. J. Chemical basis for enzyme catalysis. *Biochemistry* **2000**, *39* (21), 6267-6274.

(21) Pallotta, M. T.; Rossini, S.; Suvieri, C.; Coletti, A.; Orabona, C.; Macchiarulo, A.; Volpi, C.; Grohmann, U. Indoleamine 2,3-Dioxygenase 1 (IDO1): an Up-to-Date Overview of an Eclectic Immunoregulatory Enzyme. *FEBS J.* **2021**, 1-20.

(22) Prendergast, G. C.; Smith, C.; Thomas, S.; Mandik-Nayak, L.; Laury-Kleintop, L.; Metz, R.; Muller, A. J. Indoleamine 2,3-Dioxygenase Pathways of Pathogenic Inflammation and Immune Escape in Cancer. *Cancer Immunol. Immunother.* **2014**, *63* (7), 721-735.

(23) Moon, Y. W.; Hajjar, J.; Hwu, P.; Naing, A. Targeting the Indoleamine 2,3-Dioxygenase Pathway in Cancer. *J. Immunother. Cancer* **2015**, *3* (51).

(24) Moffett, J. R.; Namboodiri, M. A. Tryptophan and the Immune Response. *Immunol. Cell Biol.* **2003**, *81* (4), 247-265.

(25) Jensen, S. C.; Sullivan, B.; Hartzler, D. A.; Pushkar, Y. DIY XES—Development of an Inexpensive, Versatile, and Easy to Fabricate XES Analyzer and Sample Delivery System. *X-Ray Spectrom.* **2019**, *48* (5), 336-344.

(26) Glatzel, P.; Bergmann, U.; de Groot, F. M. F.; Cramer, S. P. Influence of the Core Hole on Kβ Emission Following Photoionization or Orbital Electron Capture: A Comparison using MnO and (Fe2O3)-Fe-55. *Phys. Rev. B* **2001**, *64* (4), 45109-45119.

(27) Peng, G.; deGroot, F. M. F.; Hámáláinen, K.; Moore, J. A.; Wang, X.; Grush, M. M.; Hastings, J. B.; SIddons, D. P.; Armstrong, W. H.; Mullins, O. C.; et al. High-Resolution Manganese X-ray Fluorescence Spectroscopy. Oxidation-State and Spin-State Sensitivity. *J. Am. Chem. Soc.* **1994**, *116* (7), 2914-2920.

(28) Lafuerza, S.; Carlantuono, A.; Retegan, M.; Glatzel, P. Chemical Sensitivity of Kβ and Kα X-ray Emission from a Systematic Investigation of Iron Compounds. *Inorg. Chem.* **2020**, *59* (17), 12518-12535.

(29) Gamblin, S. D.; Urch, D. S. Metal Kβ X-ray Emission Spectra of First Row Transition Metal Compounds. *J. Electron Spectros. Relat. Phenomena* **2001**, *113* (2), 179-192.

(30) Castillo, R. G.; Hahn, A. W.; Van Kuiken, B. E.; Henthorn, J. T.; McGale, J.; DeBeer, S. Probing Physical Oxidation State by Resonant X-Ray Emission Spectroscopy: Applications to Iron Model Complexes and Nitrogenase. *Angew. Chem. Int. Ed.* **2021**, *60* (18), 10112-10121.

(31) Neese, F. Importance of Direct Spin−Spin Coupling and Spin-Flip Excitations for the Zero-Field Splittings of Transition Metal Complexes: A Case Study. *J. Am. Chem. Soc.* **2006**, *128* (31), 10213-10222.

(32) Pollock, C. J.; Delgado-Jaime, M. U.; Atanasov, M.; Neese, F.; DeBeer, S. Kβ Mainline X-ray Emission Spectroscopy as an Experimental Probe of Metal–Ligand Covalency. *J. Am. Chem. Soc.* **2014**, *136* (26), 9453-9463.

(33) Lee, N.; Petrenko, T.; Bergmann, U.; Neese, F.; DeBeer, S. Probing Valence Orbital Composition with Iron Kβ X-ray Emission Spectroscopy. *J. Am. Chem. Soc.* **2010**, *132* (28), 9715-9727.

(34) Gamblin, S. D.; Urch, D. S. Metal Kβ X-ray Emission Spectra of First Row Transition Metal Compounds. *J. Electron Spectrosc.* **2001**, *113* (2), 179-192.

(35) Vankó, G.; Neisius, T.; Molnár, G.; Renz, F.; Kárpáti, S.; Shukla, A.; de Groot, F. M. F. Probing the 3d Spin Momentum with X-ray Emission Spectroscopy: The Case of Molecular-Spin Transitions. *J. Phys. Chem. B* **2006**, *110* (24), 11647-11653.

(36) Kennedy, B. J.; Brain, G.; Murray, K. S. Chlorophthalocyanine Iron(III). FePc(-2)Cl. A Spin-Admixed (S = 3/2 / S = 5/2) System. *Inorganica Chim. Acta.* **1984**, *81*, 29-31.

(37) Kennedy, B. J.; Murray, K. S.; Zwack, P. R.; Homborg, H.; Kalz, W. Spin States in Iron(III) Phthalocyanines Studied by Mössbauer, Magnetic Susceptibility, and ESR Measurements. *Inorg. Chem.* **1986**, *25* (15), 2539-2545.

(38) Dale, B. W.; Williams, R. J. P.; Johnson, C. E.; Thorp, T. L. S = 1 Spin State of Divalent Iron. I. Magnetic Properties of Phthalocyanine Iron (II). *J. Chem. Phys.* **1968**, *49* (8), 3441-3444.

(39) Evangelisti, M.; Bartolome, J.; de Jongh, L. J.; Filoti, G. Magnetic Properties of α-Iron(II) Phthalocyanine. *Phys. Rev. B* **2002**, *66* (14), 4410-4421.

(40) Davydov, R. M.; Chauhan, N.; Thackray, S. J.; Anderson, J. L. R.; Papadopoulou, N. D.; Mowat, C. G.; Chapman, S. K.; Raven, E. L.; Hoffman, B. M. Probing the Ternary Complexes of Indoleamine and Tryptophan 2,3-Dioxygenases by Cryoreduction EPR and ENDOR Spectroscopy. *J. Am. Chem. Soc.* **2010**, *132* (15), 5494-5500.

(41) Papadopoulou, N. D.; Mewies, M.; McLean, K. J.; Seward, H. E.; Svistunenko, D. A.; Munro, A. W.; Raven, E. L. Redox and Spectroscopic Properties of Human Indoleamine 2,3-Dioxygenase and a His303Ala Variant: Implications for Catalysis. *Biochemistry* **2005**, *44*, 14318-14328.

(42) Sugimoto, H.; Oda, S.; Otsuki, T.; Hino, T.; Yoshida, T.; Shiro, Y. Crystal Structure of Human Indoleamine 2,3-Dioxygenase: Catalytic Mechanism of O2 Incorporation by a Heme-Containing Dioxygenase. *Proc. Natl. Acad. Sci.* **2006**, *103* (8), 2611-2616.

(43) Luo, S.; Xu, K.; Xiang, S.; Chen, J.; Chen, C.; Guo, C.; Tong, Y.; Tong, L. High-Resolution Structures of Inhibitor Complexes of Human Indoleamine 2,3-Dioxygenase 1 in a New Crystal Form. *Acta Crystallogr. F Struct. Biol. Commun.* **2018**, *74* (11), 717-724.

(44) Terentis, A. C.; Thomas, S. R.; Takikawa, O.; Littlejohn, T. K.; Truscott, R. J.; Armstrong, R. S.; Yeh, S. R.; Stocker, R. The Heme Environment of Recombinant Human Indoleamine 2,3-Dioxygenase. *J. Biol. Chem.* **2002**, *277* (18), 15788-15794.

(45) Solovyev, M.; Kucheryavy, P.; Lockard, J. V. Local Coordination and Electronic Structure Ramifications of Guest-Dependent Spin Crossover in a Metal-Organic Framework: A Combined X-ray Absorption and Emission Spectroscopy Study. *Inorg. Chem.* **2022**, *61* (24), 9213-9223.

(46) Sono, M.; Taniguchi, T.; Watanabe, Y.; Hayaishi, O. Indoleamine 2,3-Dioxygenase: Equilibrium Studies of the Tryptophan Binding to the Ferric, Ferrous, and CO-Bound Enzymes. *J. Biol. Chem.* **1980**, *255* (4), 1339-1345.

(47) Mirgaux, M.; Leherte, L.; Wouters, J. Influence of the Presence of the Heme Cofactor on the JK-Loop Structure in Indoleamine 2,3-Dioxygenase 1. *Acta Crystallogr. D Struct. Biol.* **2020**, *76* (Pt 12), 1211-1221.

(48) Mirgaux, M.; Leherte, L.; Wouters, J. Temporary Intermediates of L-Trp Along the Reaction Pathway of Human Indoleamine 2,3-Dioxygenase 1 and Identification of an Exo Site. *Int. J. Tryptophan Res.* **2021**, *14*, 1-11.

(49) Yonetani, T.; Anni, H. Yeast Cytochrome c Peroxidase. Coordination and Spin States of Heme Prosthetic Group. *J. Biol. Chem.* **1987**, *262* (20), 9547-9554.

(50) Khubbutdinov, R.; Menushenkov, A. P.; Vartanyants, I. A. Coherence Properties of the High-Energy Fourth-Generation X-Ray Synchrotron Sources. *J. Synchrotron Radiat.* **2019**, *26* (6), 1851-1862.

(51) Shin, S. New Era of Synchrotron Radiation: Fourth-Generation Storage Ring. *AAPPS Bulletin* **2021**, *31* (1), 1-16.